Deep Mining 2024 – P Andrieux & D Cumming-Potvin (eds)

doi:10.36487/ACG_repo/2465_73

The strength of massive to moderately jointed hard rock masses for tunnel and pillar designs

Navid Bahrani [a,*], Soheil Sanipour [b], Farzaneh Hamediazad [c]

[a] *Department of Civil and Resource Engineering, Dalhousie University, Canada*

[b] *WSP, Canada*

[c] *BBA Consultants, Canada*

Abstract

This paper presents the results of a series of numerical studies conducted to simulate the damage process and failure of hard rock masses and to estimate their strength for the design of underground excavations. In these studies, the numerical models were calibrated against an empirical brittle failure criterion, commonly known as the S-shaped criterion, in order to replicate the damage evolution leading to the failure of massive to moderately jointed hard rock masses. It is demonstrated that the models calibrated to rock mass strength using the S-shaped criterion realistically replicate the failure around a test tunnel and within slender pillars under compressive and shear loading conditions. However, they tend to overestimate the strength of wide pillars compared to the empirical pillar strength database. When calibrated against the strength of pillars from the database, the models significantly underestimate the confined rock mass strength compared to the S-shaped criterion and the GSI-based Hoek–Brown failure criterion.

Keywords: r*ock mass strength, brittle failure, tunnel design, pillar design, S-shaped failure envelope*

1 Introduction

Estimating the rock mass strength is a crucial step in the design of surface and underground infrastructures. In greenfield projects, the design heavily relies on engineering judgement and assumptions regarding rock mass conditions, primarily based on limited information and data obtained from nearby sites, exploratory boreholes, core logging campaigns, and limited laboratory testing. A reliable estimation of the rock mass strength at this stage could lead to significant cost savings during the construction phase. The first step in estimating rock mass strength is to obtain intact rock strength from laboratory testing. In mining projects, two common laboratory tests conducted on intact rock are the unconfined compressive strength (UCS) and point load tests. These tests provide estimates of intact rock strength under an unconfined compressive condition. Some projects may also include Brazilian tensile tests as well as confined compression tests, although they are limited to confining pressures in the order of a few megapascals (i.e. up to σ_3 = UCS/10). Only in critical and sensitive projects, such as deep geological repositories (DGR), is rock strength obtained for a wider range of confinement (i.e. up to σ_3 = UCS/2).

Once the intact rock strength is established, empirical approaches are typically used to estimate the rock mass strength. These approaches have been developed mostly based on observations of rock mass behaviour surrounding underground openings where confinement is relatively low. Therefore, these methods are more suited for the design of tunnel, stopes, and slender pillars. However, for wide pillars where the confining pressure at the core could reach to magnitudes as high as the far-field minimum principal stress (especially in deep mines), the rock mass strength must be determined for a wide range of confinement (e.g. σ_3 = 0 to UCS/2).

* Corresponding author. Email address: navid.bahrani@dal.ca

It is known that conventional rock mass strength estimation approaches, such as the shear-based Hoek–Brown (HB) failure criterion with its strength parameters obtained from the GSI system (Hoek and Brown, 2019), do not accurately estimate the strength of massive to moderately jointed rock masses with GSI values greater than 65 (Cai et al. 2004; Valley et al. 2011; Bahrani & Kaiser 2020). To overcome this limitation, Diederichs (2003) proposed an S-shaped strength envelope originating from earlier work by Martin et al. (1999), who proposed the HB brittle parameters for estimating the depth of failure around underground openings in hard rocks. While the S-shaped failure criterion has not yet been implemented in commercial numerical software programs, other forms of this criterion, such as cohesion weakening and frictional strengthening (CWFS) and damage initiation and spalling limit (DISL), have been successfully used in several tunnelling projects to predict or replicate the depth and shape of failure. These approaches, however, do not lead to capturing the excavation damage zone (EDZ) – a critical design parameter for DGRs – as they have primarily been developed for use in continuum models where the rock mass is simulated as a homogeneous medium.

The S-shaped failure criterion estimates the rock mass strength envelope across various confinement levels (σ_3 = 0 to UCS/2), but its applicability to high confinement problems, such as the strength estimation and design of wide pillars (width-to-height ratios of 1 to 2.5), has not been verified. This paper presents a series of studies investigating the applicability of the S-shaped failure criterion for predicting brittle failure and estimating rock mass strength for tunnel and pillar designs. For this purpose, continuum-based heterogeneous models were initially used to replicate brittle damage leading to failure around a test tunnel and within slender mine pillars. Next, the results of a study with discontinuum-based heterogeneous models were employed to assess the applicability of this criterion for estimating the strength of hard rock pillars with a wide range of width-to-height ratios (i.e. confinement). The outcomes of these studies provide insights into the strength of massive to moderately jointed hard rock masses necessary for designing tunnels and pillars in hard rock under high-stress conditions.

2 Strength estimation of massive to moderately jointed hard rock masses

According to Diederichs (2003), the in situ rock strength at low confinement (i.e. near excavation boundary) in massive to moderately jointed hard rock masses (with GSI > 65) under high-stress conditions ($0.15 < \sigma_1 / UCS < 0.4$) can be estimated by the damage initiation threshold defined by the HB brittle parameters (i.e. s = 0 and m = 0.11). At high confinement, where the rock fails in shear, the strength is equal to the laboratory crack damage threshold or the long-term strength of intact rock. The transition in the strength from low to high confinement defines the spalling limit ranging from σ_1/σ_3 = 10 to 20. Figure 1a shows the S-shaped failure envelope proposed by Diederichs (2003) along with anticipated failure modes of hard brittle rocks under different in situ stress states.

More recently, Bewick et al. (2019) proposed a tri-linear strength envelope and its equivalent Hoek–Brown envelope to expand this criterion for rock masses with various intact rock conditions. Figure 1b shows the lower and upper bounds of the tri-linear strength envelope. The main components of the tri-linear envelope are:

1. spalling strength, which is between 30 and 50% of the intact rock UCS
2. spalling limit ($10 < \sigma_1/\sigma_3 < 20$; Kaiser et al. 2000; Diederichs 2003)
3. confined rock mass strength, which is approximately 70 to 90% of the laboratory peak strength of intact rock (Bewick et al. 2019).

Bewick et al. (2019) suggested that the tri-linear strength envelope can be approximated using an 'equivalent' HB strength envelope for use in commercially available numerical programs. An example of the equivalent HB strength envelope for a rock mass with an intact rock UCS of 230 MPa and an m_i of 22 is presented in Figure 1b. This envelope was determined by adjusting the GSI and slope of the envelope in a way that the HB curve would intersect the y-axis at the spalling strength of 0.3 × 230 = 69 MPa and end at the intersection of σ_1/σ_3 = 6 and the confined rock mass strength (i.e. 80% of laboratory peak strength) by passing through the spalling limits ($10 < \sigma_1/\sigma_3 < 20$).

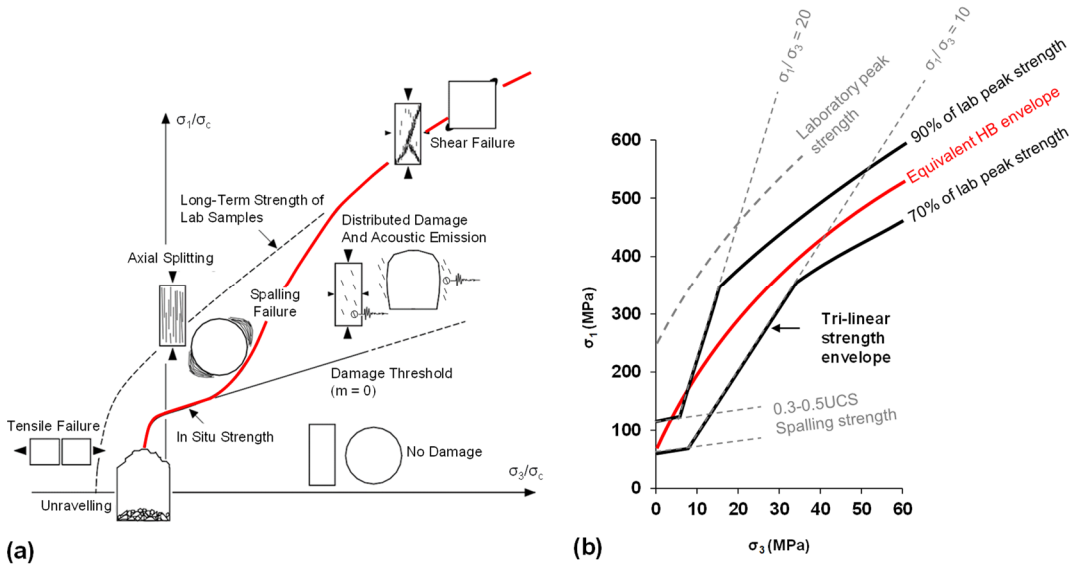

Figure 1 **(a) Schematic of the S-shaped failure envelope for brittle rocks illustrating different failure modes for massive to moderately jointed rock masses: no damage, unravelling, spalling and shear failure (after Diederichs 2003); (b) Upper and lower bounds of the tri-linear strength envelope comprised of spalling strength, spalling limit and long-term laboratory peak strength along with the equivalent Hoek–Brown (HB) failure envelope (Hamediazad & Bahrani 2024)**

3 Simulation of brittle failure around tunnels and pillars

In this section, the application of the tri-linear and the equivalent HB strength envelopes for replicating brittle damaged and failure around a test tunnel and within hard rock pillars under shear and compressive loading conditions are investigated.

3.1 V-shaped notch failure around a test tunnel

The brittle failure around the mine-by experiment (MBE), which was a 3.5-m diameter circular tunnel at the Underground Research Laboratory (URL) in Manitoba, Canada, has been the subject of several studies in the past few decades. The MBE tunnel was excavated in massive Lac de Bonnet (LdB) granite at the 420 Level of the URL to investigate the rock mass response to excavation. Laboratory tests conducted on intact specimens of LdB granite yield an average UCS of about 213 MPa, a direct tensile strength of 6.9 MPa and an m_i of 28. A v-shaped notch failure was formed during the construction of the MBE tunnel (Figure 2) even though the maximum tangential stress calculated from the Kirsch equation (i.e. 3 × 60 – 11 = 169 MPa) is much less than the intact rock UCS.

Figure 2 **V-shaped notch failure around the mine-by experiment tunnel at 420 Level of the URL (after Read et al. 1998)**

Commonly known approaches in continuum model used to simulate the failure around the MBE tunnel include the CWFS by Hajiabdolmajid et al. (2002) and the DISL by Diederichs (2003). While these methods showed success in simulating the depth and shape of failure, they do not capture the extent of the EDZ, which is defined as a zone around an excavation characterised by stress-induced microcracks.

Sanipour et al. (2022) developed a heterogeneous model in RS2 (by Rocscience Inc) by dividing the homogeneous domain into several nonoverlapping convex polygonal (Voronoi) blocks (Figure 3a) to simulate the v-shaped notch and the EDZ monitored around the tunnel using microseismic events. The blocks in this model, referred to as the Voronoi tessellated model (VTM), were meshed with six-noded triangular elements. The block boundaries were simulated using the built-in the joint elements which are four-noded quadrilateral elements. Sanipour et al. (2022) calibrated the VTM to the rock mass strength estimated using both the equivalent HB and tri-linear envelopes described in the previous section. Figure 3b shows the emergent strength envelope obtained from the RS2-VTM calibrated to the tri-linear envelope. The results illustrate that the envelope starts from the crack initiation stress level of LdB granite at low confinement ($\sigma_3 < 5$ MPa), follows the spalling limit range up to a confining pressure of about 30 MPa, and reaches the long-term strength of LdB granite at high confining pressures (i.e. $\sigma_3 = 40$ to 60 MPa).

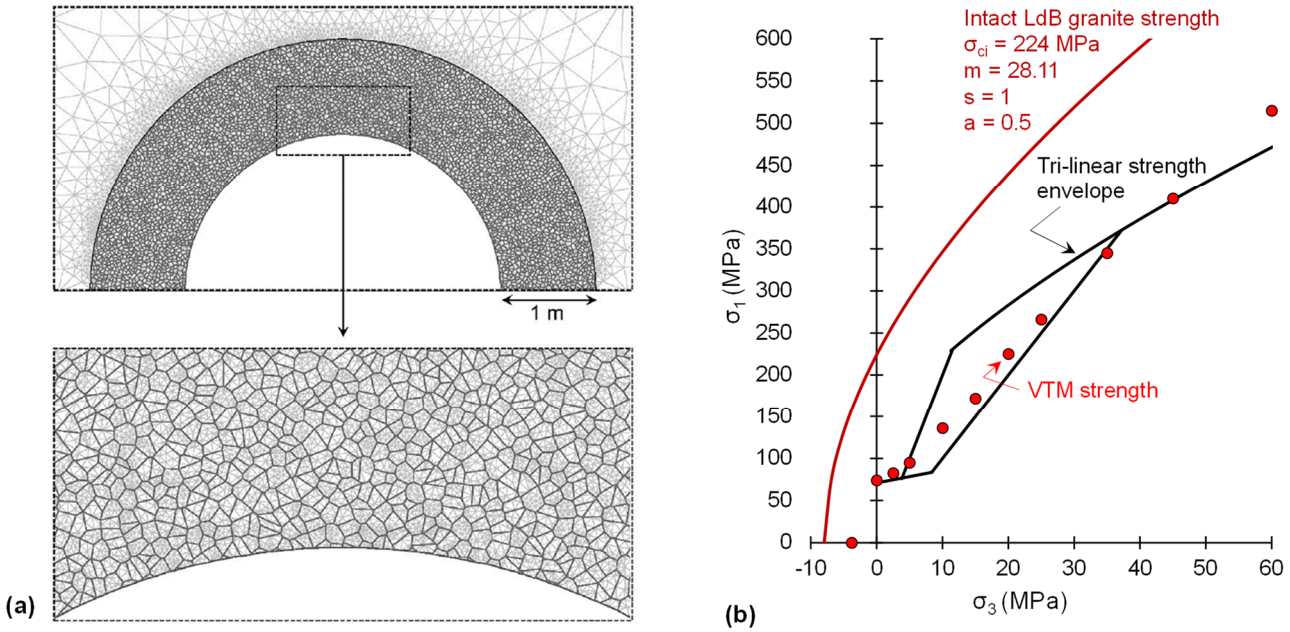

Figure 3 (a) RS2-VTM of the MBE tunnel consisting of a homogeneous domain far from the excavation and a heterogeneous domain consisting of Voronoi blocks around the tunnel perimeter; (b) Peak strength of VTM calibrated to the tri-linear envelope for LdB granite (Sanipour et al. 2022)

A comparison between the depth and shape of failure around the MBE tunnel and those replicated by the RS2-VTMs calibrated to the equivalent HB and tri-linear envelopes are presented in Figure 4. This figure clearly shows that even though the UCS of both envelopes are equal, the VTM calibrated to the tri-linear envelope better captures the depth and shape of failure. The VTM calibrated to the equivalent HB envelope underestimates the depth of failure and overestimates the extent of failure at the two sides of the notch region (Figure 4b). However, the VTM calibrated to the tri-linear envelope successfully captures both the depth and shape of failure around the MBE tunnel (Figure 4c). Additionally, the extent of block boundary yielding indicating damage is consistent with the recorded microseismic events (compare Figures 4a and 4c).

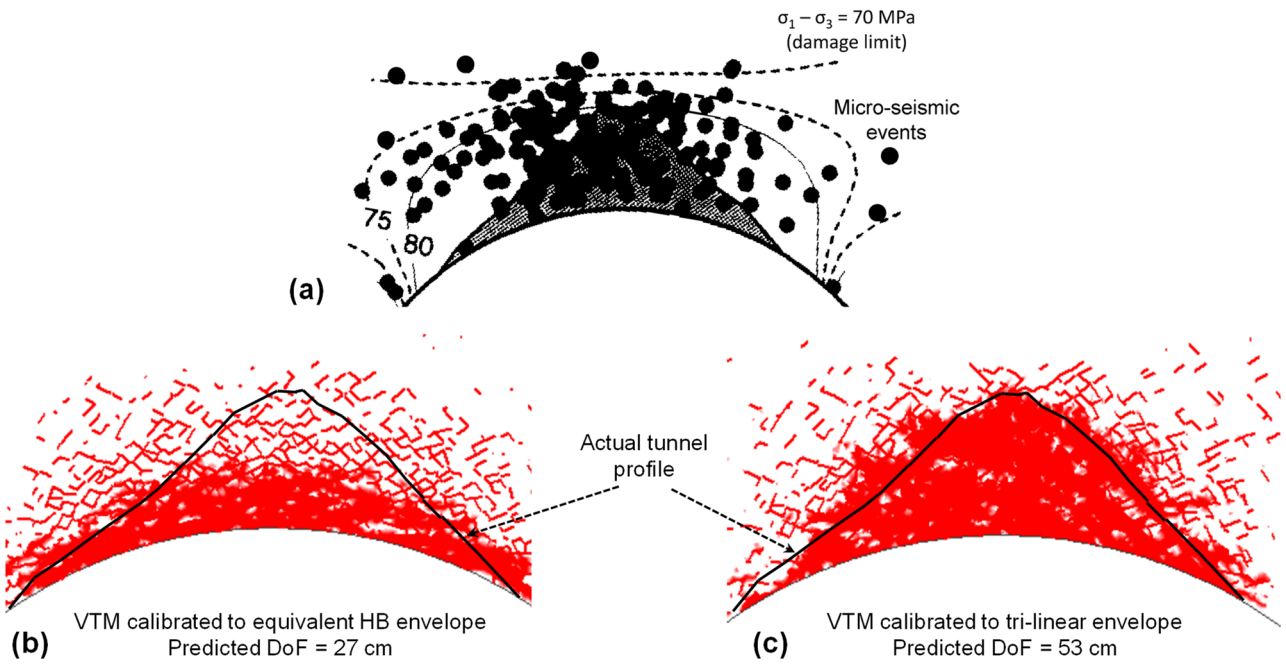

Figure 4 (a) Failure profile and microseismic events indicating damage around the MBE tunnel (Martin 1997). Simulated failure and damage using RS2-VTMs calibrated to (b) equivalent Hoek–Brown (HB) envelope and (c) tri-linear envelope (Sanipour et al. 2022)

The difference in simulation results (Figures 4b and 4c) between the two scenarios can be attributed to the variations in strength as a function of confinement. The model calibrated to the tri-linear envelope can experience damage and failure at lower confinement levels, whereas the HB model cannot. This difference in strengths based on confinement is illustrated in Figure 3b.

3.2 Failure of pillars under compressive and shear loading conditions

The Quirke Mine is an abandoned uranium mine located in the Elliot Lake district, Ontario, Canada. The rib pillars in this mine were initially laid out with their long axes parallel to the dip direction of the orebody with a dip angle of 20°. In the central part of the mine, the pillars were re-oriented at 45° to the orebody dip direction. This realignment resulted in adverse shear loading within the pillars that led their failure. Two examples pillar failure in the Elliot Lake district are shown in Figure 5.

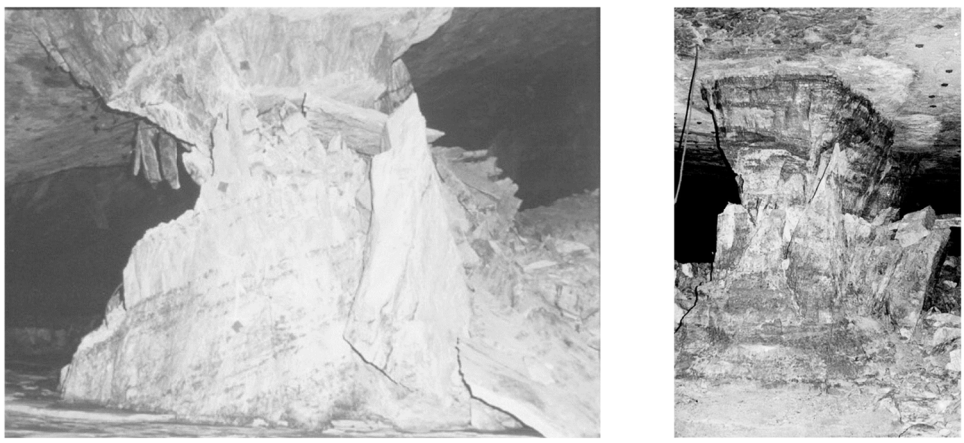

(a) (b)

Figure 5 Examples of crushed pillars at the Elliot Lake district. (a) Pillar under shear (Martin & Maybee 2000); (b) Pillar under compression (Rafiei Renani & Martin 2018)

The intact rock (quartzite) at the Quirke Mine has a UCS of 230 MPa and an m_i of 22. The rock mass is massive to moderately jointed, by a GSI of 80 (Martin and Maybee, 2000). Hamediazad & Bahrani (2022) used a heterogeneous model in RS2 consisting of Voronoi blocks similar to the model described in the previous section. They calibrated the RS2-VTM to a deformation modulus of 60 GPa and the equivalent HB strength envelope (Figure 1b). Figure 6a shows the results of model calibration compared to the laboratory peak strength and the estimated rock mass strength based on the tri-linear and its equivalent HB approaches. The calibrated VTM was then used in a series of simulations to investigate the strength and failure mechanism of the pillars subjected to compressive and shear loading conditions. As illustrated in Figure 6b, the pillar with a W/H of 0.75 was simulated as a heterogeneous material consisting of Voronoi blocks, while the host rock was simulated as an elastic homogenous material within the stress regime consistent with the Elliot Lake area (σ_{Hmax} = 28, σ_{hmin} = 19.5, σ_v = 13.5 MPa; Hedley et al. 1984). The initial simulations were conducted for pillars with a W/H of 0.75.

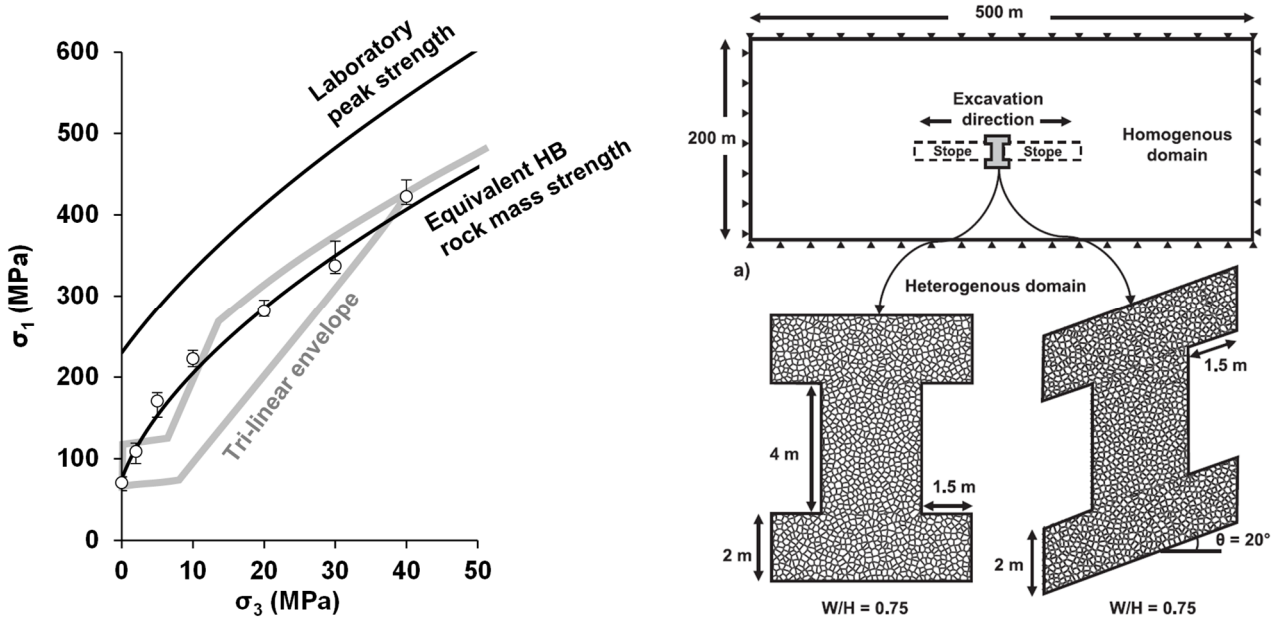

Figure 6 (a) Compressive strengths of the calibrated RS2-VTM compared to the tri-linear and its equivalent HB strength envelopes; (b) RS2 models of Quirke Mine pillars with a W/H of 0.75 consisting of heterogeneous and homogeneous domains (Hamediazad & Bahrani 2022)

The pillar loading was simulated in two stages. First, two parallel drifts with a diameter of 4.5 m were excavated. The pillars were further loaded by gradually excavating the stopes at both sides until they failed. The stress-strain curves of both pillars illustrated in Figure 7a indicate that the strength of the pillar in shear is lower than that in compression. Figure 7b shows the failure mode the two pillars, suggesting that tensile yielding is the dominant mode of failure. In the modelled pillar in compression, the yielding pattern is relatively symmetrical. The pillar in shear, however, begins to yield from the opposite corners. The yielding is then progressively extended diagonally to the core. The overall failure mode of both modelled pillars is consistent with field observations at the Elliot Lake district (Figure 5).

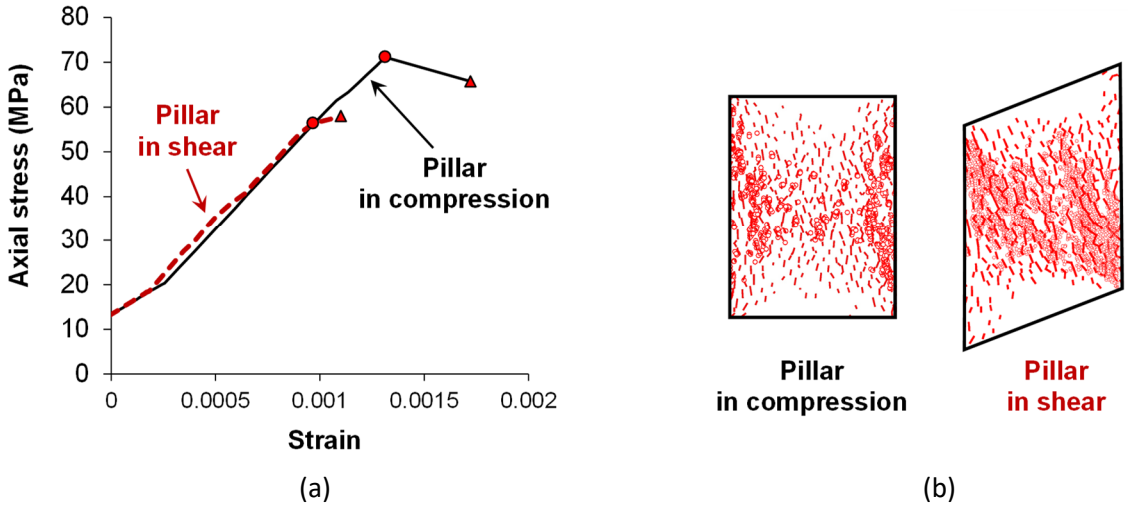

Figure 7 (a) Stress-strain curves; (b) Failure modes of modelled Quirke Mine pillars in shear and compression simulated using calibrated VTM in RS2 (Hamediazad & Bahrani 2022)

More recently, Hamediazad & Bahrani (2024) further investigated the influence of W/H on the strength of pillars in compression and shear. They considered pillars with W/H of 0.5, 1, and 1.5 in their simulations to cover the typical pillar sizes at the Quirke Mine. Figure 8a shows the normalised peak strengths of the pillars in compression and shear added to the hard rock pillar strength database developed by Lunder (1994) and the Elliot Lake district pillar database (Hedley & Grant 1972). This figure shows that the simulation results for the pillars with W/H of 0.5 and 0.75 are in reasonable agreement with those reported by Lunder (1994). The strength of the modelled pillars with a W/H of 1 is also consistent with the data obtained from the Elliot Lake district.

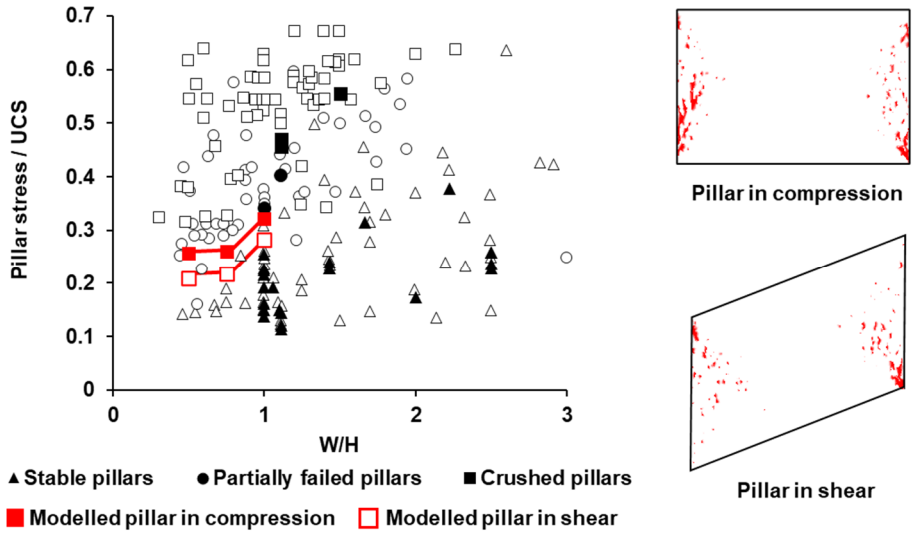

Figure 8 (a) Pillar stability curves for modelled pillars in compression and shear compared to the hard rock pillar strength database (white solid symbols) by Lunder (1994). Black solid symbols represent pillar cases at the Elliot Lake district reported by Hedley and Grant (1972); (b) Yielded elements in modelled pillars with a W/H of 1.5 (Hamediazad & Bahrani 2024)

Hamediazad & Bahrani (2024) found that the modelled pillars with a W/H of 1.5 did not fail even with an extraction ratio greater than 90%, whereas pillars of similar sizes failed at the Elliot Lake district (black square symbols in Figure 8a). Figure 8b shows the yielded pattern within the pillar with a W/H of 1.5 indicating that the core remains intact in both pillars. This suggests that the strength of the modelled pillar with a W/H of

1.5 might have been overestimated. Hamediazad & Bahrani (2024) discussed that the reason behind this overestimation could be due to the rock mass strength envelope (i.e. equivalent HB), which tends to overestimate the tri-linear strength envelope at low confinement, inhibiting failure propagation to the confined region of the pillar (i.e. core).

4 Back-analysis of the rock mass strength

Hamediazad & Bahrani (2024) concluded that although the 2D continuum-based VTM reasonably captured the overall behaviour of slender pillars under different loading conditions at relatively low computation time. It should be highlighted that the models were unable to capture the anticipated post-peak response. This can be attributed to the fact that the finite element method does not explicitly capture fracturing, block detachment and associated stress redistribution past the peak stress. Furthermore, they concluded that the strength of wide pillars was likely overestimated in their study. To overcome these limitations, they used the discontinuum program 3DEC and its bonded block modelling (BBM) approach. Figure 9 shows the geometry and boundary conditions of the plane strain model of a pillar with a W/H of 0.75 generated in 3DEC. In this model, the host rock is a homogeneous elastic material with a deformation modulus of 60 GPa and a Poisson's ratio (v) of 0.2. The pillar and the surrounding rock mass were simulated as an assembly of Voronoi block bonded together at their contacts. The pillar was loaded from zero stress until failure by applying a constant vertical velocity on the top model boundary, as illustrated in Figure 9.

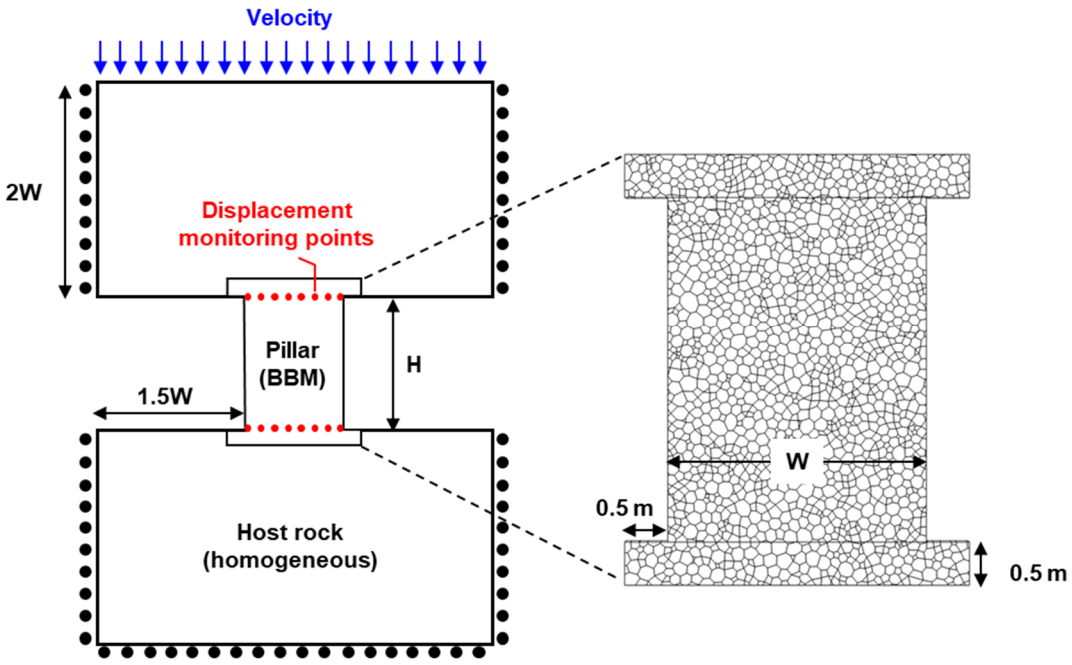

Figure 9 3DEC model geometry and boundary conditions used to simulate hard rock pillar failure (Hamediazad & Bahrani 2024)

In the first series of model calibration, Hamediazad & Bahrani (2024) generated an inelastic BBM in which the CWFS behaviour was used for both zones inside the blocks and the contacts. In this model, the blocks were allowed to yield, meaning that in addition to E and v, required for the zones inside the blocks, the peak and residual strengths and the plastic shear strain (e^{ps}) had to be defined. Fracturing was explicitly simulated as contact (or block boundary) failure. Hamediazad & Bahrani (2024) calibrated the BBM against the lower bound of the tri-linear strength envelope (Figure 1b). The calibration results, presented in Figure 10a, indicate that the emergent strength envelope of the BBM is an S-shaped curve. Once the BBM was calibrated, its micro-properties were used in the pillar model to investigate the strength and failure mechanism of hard rock pillars as a function of W/H ratio. Following the geometry and boundary conditions illustrated in Figure 9, pillars with W/H ratios of 0.5, 0.75 and 1 were created. Figure 10b presents the stress-strain response of these pillars.

As shown in Figure 10b, although the post-peak response of the pillar with a W/H of 0.5 is consistent with those in previous studies (e.g. Rafiei Renani & Martin 2018; Sinha & Walton 2018; Li et al. 2019), wider pillars (W/H > 0.5) exhibit hardening behaviour. Figure 10c shows the normalised peak strengths for the modelled pillars compared to the pillar strengths from the Elliot Lake district (Hedley & Grant 1972) and the hard rock pillar strength database (Lunder 1994), respectively. It is evident from these figures that the inelastic BBM calibrated to the tri-linear strength envelope overestimates the strength of pillars with W/H ratios of 0.75 and 1. In other words, most of the failed pillar cases in the database fall below the estimated pillar strengths for the pillar W/H of 0.75 and 1.

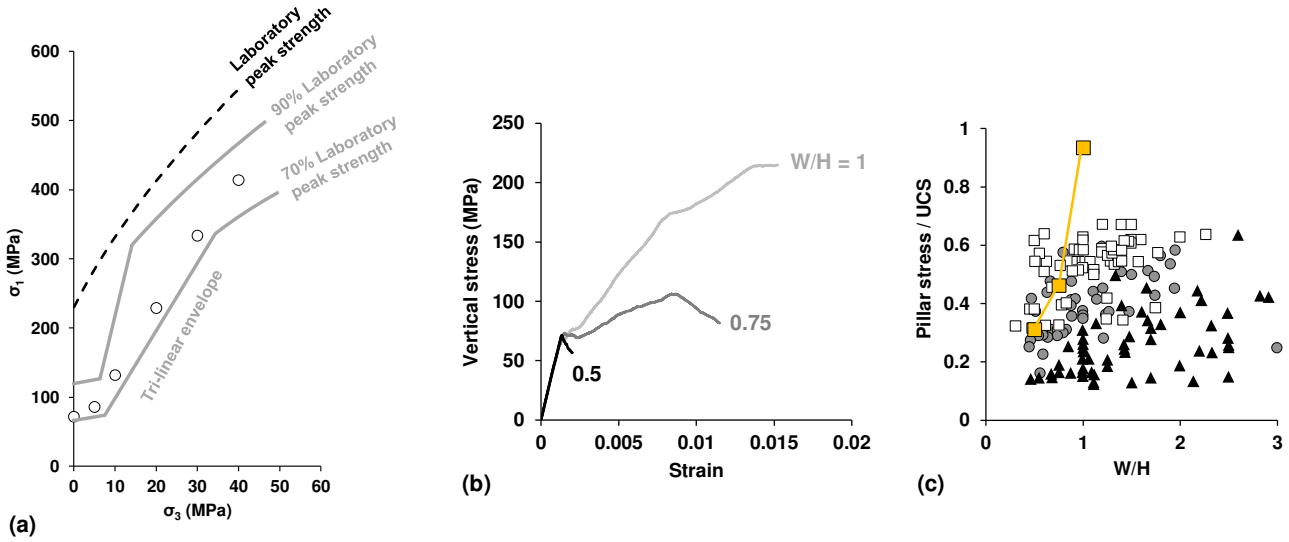

Figure 10 (a) Peak compressive strengths of calibrated inelastic BBM compared to the lower and upper bounds of the tri-linear strength envelope; (b) Stress–strain curves of the pillars with W/H of 0.5, 0.75 and 1 generated with the calibrated inelastic BBM; (c) Comparison of estimated pillar strength with empirical pillar strength database (Lunder 1994; Hamediazad & Bahrani 2024)

Hamediazad & Bahrani (2024) reported that no single set of micro-properties could be found to match both the tri-linear strength envelope and the pillar strength data with a more realistic post-peak behaviour for pillars with W/H of 0.75 and 1. This led to the second series of model calibration. In the second attempt, they calibrated the pillar model to the empirical pillar strength data and the expected pillar post-peak behaviour. For this purpose, the shear strength parameters of the BBM in the pillar had to be adjusted iteratively. Hamediazad & Bahrani (2024) found that acceptable results were obtained when the contacts were assigned lower residual cohesion and friction angle than their peak values. This behaviour is referred to as the cohesion-weakening and friction-weakening (CFW). In this model, the zones inside the blocks were assigned the CWFS behaviour.

Figure 11a presents the stress-strain curves for modelled pillars with the W/H ratios of 0.5 to 2 obtained from this calibration strategy. The stress-strain curves demonstrate brittle response for the W/H of 0.5 and strain softening for the W/H of 0.75 and 1. The wider pillars (W/H = 1.5 & 2) exhibit a strain-hardening response, which is consistent with those in other numerical studies (e.g. Rafiei Renani & Martin 2018; Sinha & Walton 2018, 2019). Figure 11b depicts the pillar stability curve obtained from this study compared to the empirical pillar strength data. It is evident that the stability curve from this study is consistent with the database. Hamediazad & Bahrani (2024) also reported that their stability curve is comparable to that of Martin & Maybee (2000), who used continuum elastic models with the HB brittle parameters.

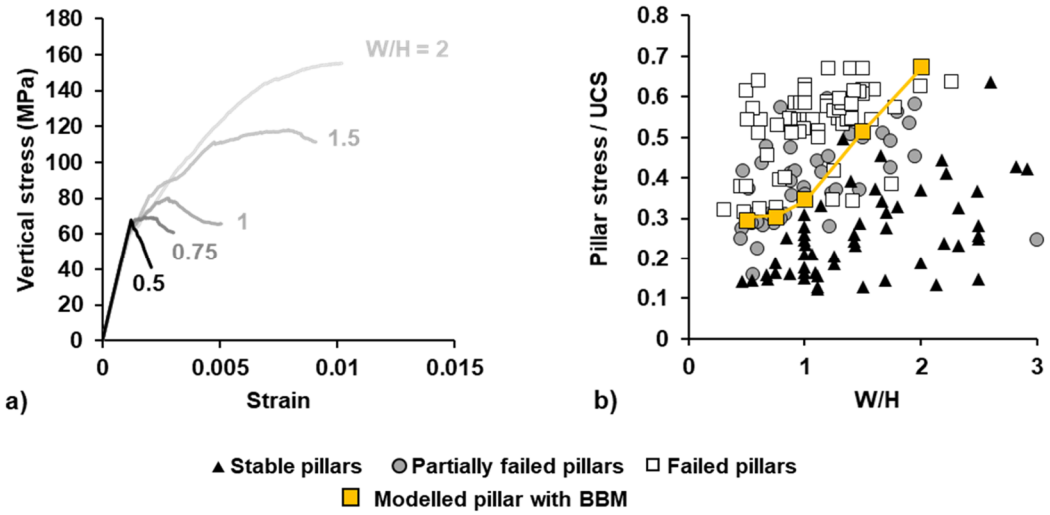

Figure 11 Simulation results for pillars with W/H of 0.5 to 2 using the revised BBM with CWFS behaviour for blocks and CFW behaviour for contacts. (a) Stress-strain curves; (b) Normalised peak strength compared to database by Lunder (1994) and Hamediazad & Bahrani (2024)

Once the strength of the modelled pillar was validated against the empirical pillar strength database and the post-peak response, its micro-properties were used in a series of unconfined and confined compression tests to back-analyse the rock mass strength. Figure 12 shows the peak and residual rock mass strength envelopes for the revised inelastic BBM. This figure demonstrates that the back analysed peak strength envelope is linear, whereas the residual envelope is bi-linear and has a higher initial slope compared to the peak envelope. Furthermore, at low confinement ($\sigma_3 < 10$ MPa), the strength of the revised inelastic BBM is close to the lower bound of the tri-linear envelope, defined by the laboratory crack initiation or in situ damage initiation threshold. Surprisingly, the back-analysed rock mass strength underestimates the tri-linear strength envelope and the conventional HB strength envelope with a GSI of 80 at higher confining pressures ($\sigma_3 \geq 10$ MPa); it exhibits a shallower rock mass strength envelope ($\sigma_1/\sigma_3 = 3.5$) than the tri-linear envelope.

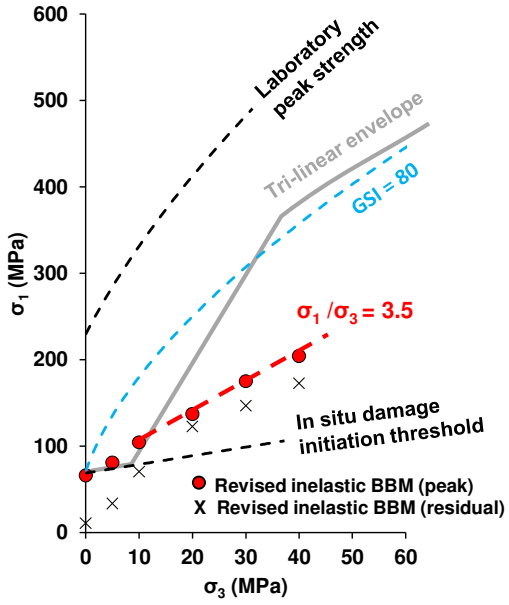

Figure 12 Back-analysed peak and residual strengths of the rock mass from the revised inelastic BBM (with CWFS behaviour for blocks and CFW behaviour for contacts) compared to the tri-linear envelope, the HB envelope with GSI of 80, and the in situ damage initiation threshold (Hamediazad & Bahrani 2024)

Figure 13 illustrates the failure modes of the revised calibrated pillar models (with CWFS behaviour for blocks and CFW behaviour for contacts) with different pillar W/H, respectively. This figure shows that the failure in pillars with W/H ratios of 0.5 and 1 is dominated by tensile cracking and intra-block tensile yielding, which initiates from the pillar walls and propagates towards the core. As the W/H increases, spalling and block detachment near the pillar walls allows the damage to propagate to the pillar core, which eventually led to the shear failure of the pillar core. Note that this combined failure mechanism in pillars cannot be captured in conventional continuum models, where the rock mass is simulated as a homogeneous material.

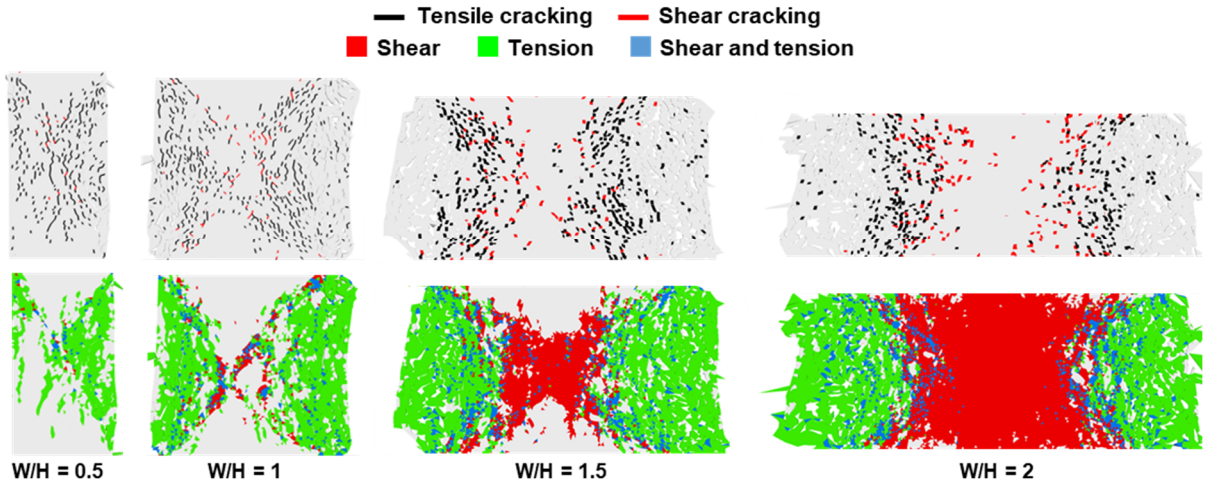

Figure 13 Failure mode of pillar models (with CWFS behaviour for blocks and CFW behaviour for contacts) at the post-peak stage for different pillar W/H (Hamediazad & Bahrani 2024)

5 Conclusion

The estimation of rock mass strength is vital for designing both surface and underground infrastructures. Traditionally, this estimation relies heavily on empirical approaches, which may lack accuracy especially for high-stress conditions. Conventional methods such as the Hoek–Brown criterion struggle to accurately predict the strength of massive to moderately jointed hard rock masses primarily due to the origin of the data used to develop such criteria. An alternative approach is to consider an S-shaped or tri-linear strength envelope that treats the rock mass strength differently by assuming a lower strength at low confining regions.

This study investigated the applicability of the S-shaped failure criterion for predicting brittle failure and estimating rock mass strength for tunnel and pillar designs. Using the VTM multiple scenarios including brittle damage and failure simulation around a test tunnel were explored, along with pillar strength under various loading conditions.

The simulation results suggest that the S-shaped failure criterion particularly when calibrated to the tri-linear strength envelope, offers improved accuracy in predicting brittle failure compared to conventional methods. This was evident in simulations of tunnel failure modes and slender pillar behaviours under compressive and shear loading. Further simulations using a discontinuum-based modelling approach were carried out to back-analyse the rock mass strength for the design of pillars with a wider range of width-to-height ratios. It was found that the pillar models were calibrated against the trend observed in the empirical pillar strength database, the back analysed rock mass strength underestimated the peak rock mass strengths estimated using the tri-linear and the HB envelopes, while it overestimated the damage initiation threshold for massive to moderately jointed hard rock masses.

These investigations emphasise the significance of accounting for a range of influencing factors in design, particularly confinement and rock mass conditions, essential for accurately estimating rock mass strength in infrastructure design. Further research is needed to refine modelling techniques, assumptions and improve our understanding of rock mass behaviours under different loading conditions.

Acknowledgement

This research was supported by the Natural Sciences and Engineering Research Council of Canada, Rocscience Inc., and Dalhousie University.

References

Bahrani, B, & Kaiser, PK 2020, 'Influence of degree of interlock on confined strength of jointed hard rock masses', *Journal of Rock Mechanics and Geotechnical Engineering*, vol. 12, no. 6, pp. 1152–1170.

Bewick, RP, Kaiser, PK, & Amann, F 2019, 'Strength of massive to moderately jointed hard rock masses', *Journal of Rock Mechanics and Geotechnical Engineering*, vol. 11, no. 3, pp. 562–575.

Cai, M, Kaiser, PK, Uno, H, Tasaka, Y, & Minami, M 2004, 'Estimation of rock mass deformation modulus and strength of jointed hard rock masses using the GSI system', *International Journal of Rock Mechanics and Mining Sciences*, vol. 41, no. 1, pp. 3–19.

Diederichs, MS 2003, 'Manuel Rocha medal recipient rock fracture and collapse under low confinement conditions', *Rock Mechanics and Rock Engineering*, vol. 36, no. 5, pp. 339–381.

Hajiabdolmajid, V, Kaiser, PK, & Martin, CD 2002, 'Modelling brittle failure of rock', *International Journal of Rock Mechanics and Mining Sciences*, vol. 39, no. 6, pp. 731–741.

Hamediazad, F, & Bahrani, N 2022, 'Simulation of hard rock pillar failure using 2D continuum-based Voronoi Tessellated models: the case of Quirke Mine, Canada', *Computers and Geotechnics*, vol. 148, no. 104808.

Hamediazad, F, & Bahrani, N 2024, 'Evaluation of the rock mass strength for hard rock pillar design using bonded block models', *Rock Mechanics and Rock Engineering*, vol. 57, pp. 3659–3680.

Hedley, DGF, & Grant, F 1972, 'Stope-and-pillar design for the Elliot Lake Uranium Mines', *Bulletin of Canadian Institute of Mining and Metallurgy*, vol. 65, pp. 37–44.

Hedley, DGF, Roxburgh, JW & Muppalaneni, SN 1984, 'A case history of rockbursts at Elliot Lake', *Proceedings of 2nd International Conference on Stability in Underground Mining. Lexington*, American Institute of Mining. Metallurgical and Petroleum Engineers Inc, New York.

Hoek, E, & Brown, ET 2019, 'The Hoek–Brown failure criterion and GSI–2018 edition', *Journal of Rock Mechanics and Geotechnical Engineering*, vol. 11. no. 3, pp. 445–463.

Kaiser, PK, Diederichs, MS, Martin, CD, Sharp, J & Steiner, W 2000, 'Underground works in hard rock tunnelling and mining', *ISRM International Symposium*, International Society for Rock Mechanics and Rock Engineering, Lisbon.

Li, X, Kim, E & Walton, G 2019, 'A study of rock pillar behaviors in laboratory and in-situ scales using combined finite-discrete element method models', *International Journal of Rock Mechanics and Mining Sciences*, vol. 118, pp. 21–32.

Lunder, PJ 1994, *Hard Rock Pillar Strength Estimation and Applied Empirical Approach*, PhD thesis, University of British Columbia, Vancouver.

Martin, CD 1997, 'The effect of cohesion loss and stress path on brittle rock strength', *Canadian Geotechnical Journal*, vol. 34, pp. 698–725.

Martin, CD, & Maybee, WG 2000, 'The strength of hard-rock pillars', *International Journal of Rock Mechanics and Mining Sciences*, vol. 37, no. 8, pp. 1239–1246.

Martin, CD, Kaiser, PK & McCreath, DR 1999, 'Hoek-Brown parameters for predicting the depth of brittle failure around tunnels', *Canadian Geotechnical Journal*, vol. 36, no. 1, pp. 136–151.

Read, RS, Chandler, NA & Dzik EJ 1998, 'In situ strength criteria for tunnel design in highly stressed rock masses', *International Journal of Rock Mechanics and Mining Sciences*, vol. 35, no. 3, pp. 261–278.

Rafiei Renani, H & Martin, CD 2018, 'Modeling the progressive failure of hard rock pillars', *Tunnelling and Underground Space Technology*, vol. 74, pp. 71–81.

Sanipour, S, Bahrani, N & Corkum, A 2022, 'Simulation of brittle failure around Canada's Mine-By Experiment Tunnel using 2D continuum-based Voronoi tessellated models', *Rock Mechanics and Rock Engineering*, vol. 55, No. 10, pp. 6387-6408.

Sinha, S & Walton, G 2018, 'A progressive S-shaped yield criterion and its application to rock pillar behavior', *International Journal of Rock Mechanics and Mining Sciences*, vol. 105, pp. 98–109.

Sinha, S & Walton, G 2019, 'Understanding continuum and discontinuum models of rock-support interaction for excavations undergoing stress-induced spalling', *International Journal of Rock Mechanics and Mining Sciences*, vol. 123, no. 104089.

Valley, B, Kim, BH, Suorineni, FT, Bahrani, N, Bewick, R & Kaiser, PK 2011, 'Influence of confinement dependent failure processes on rock mass strength at depth', *Proceedings of ISRM Congress*, International Society for Rock Mechanics and Rock Engineering, Lisbon.